

## Accepted Article

**Title:** Discovery of new iridoids as FXR agonists from *Morinda officinalis*: Agonistic potentials and molecular stimulations

**Authors:** Zhi-Lin Luan, Fei Qiao, Wen-Yu Zhao, Wen-Hua Ming, Zhen-Long Yu, Jie Liu, Sheng-Yun Dai, Shuang-Hui Jiang, Chao-Jie Lian, Cheng-Peng Sun,\* Bao-Jing Zhang, Jian Zheng,\* Shuang-Cheng Ma,\* and Xiao-Chi Ma

This manuscript has been accepted and appears as an Accepted Article online.

This work may now be cited as: *Chin. J. Chem.* **2020**, *39*, 10.1002/cjoc.202000654.

The final Version of Record (VoR) of it [with formal page numbers](#) will soon be published online in Early View: <http://dx.doi.org/10.1002/cjoc.202000654>.

# Discovery of new iridoids as FXR agonists from *Morinda officinalis*: Agonistic potentials and molecular stimulations

Zhi-Lin Luan,<sup>a,+</sup> Fei Qiao,<sup>b,+</sup> Wen-Yu Zhao,<sup>a,+</sup> Wen-Hua Ming,<sup>a</sup> Zhen-Long Yu,<sup>a</sup> Jie Liu,<sup>b</sup> Sheng-Yun Dai,<sup>b</sup> Shuang-Hui Jiang,<sup>b</sup> Chao-Jie Lian,<sup>b</sup> Cheng-Peng Sun,<sup>\*,a</sup> Bao-Jing Zhang,<sup>a</sup> Jian Zheng,<sup>\*,b</sup> Shuang-Cheng Ma,<sup>\*,a</sup> and Xiao-Chi Ma<sup>a</sup>

<sup>a</sup> Dalian Key Laboratory of Metabolic Target Characterization and Traditional Chinese Medicine Intervention, College of Pharmacy, College of Integrative Medicine, Dalian Medical University, Dalian, China.

<sup>b</sup> National Institutes for Food and Drug Control, Beijing, China.

<sup>+</sup> These authors contributed equally to this work.

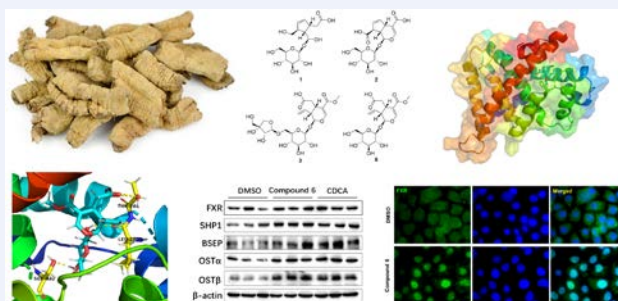
## Keywords

*Morinda officinalis* | Iridoid | FXR | Agonistic effect

## Main observation and conclusion

The investigation of *Morinda officinalis* led to the isolation of twelve compounds (**1-12**), including three new iridoid glycosides, morindalins A-C (**1-3**), and nine known compounds (**4-12**). Their structural identifications were conducted using HRMS, 1D and 2D NMR, and electronic circular dichroism (ECD) spectra as well as quantum chemical computations. Compound **6** displayed most significantly agonistic activity against farnesoid X receptor (FXR) with an EC<sub>50</sub> value of 7.18 μM, and its agonistic effect was verified through the investigation of FXR downstream target genes including small heterodimer partner 1 (SHP1), bile salt export pump (BSEP), and organic solute transporter subunit alpha and beta (OSTα and OSTβ). The potential interaction of compound **6** with FXR was analyzed by molecular docking and molecular dynamics stimulation, revealing that amino acid residues Leu287, Thr288, and Ser332 played a crucial role in the activation of compound **6** towards FXR. These findings suggested that compound **6** could be regarded as a potential candidate for the development of FXR agonists.

## Comprehensive Graphic Content



\*E-mail: zhengjian@nifdc.org.cn (J. Zheng); masc@nifdc.org.cn (S.C. Ma); suncp146@163.com (C.P. Sun).

[View HTML Article](#)

[Supporting Information](#)

## Background and Originality Content

As a member of the nuclear receptor (NR) superfamily, farnesoid X receptor (FXR; NR1H4) is mainly expressed in the liver, ileum, and kidney, and plays critical roles in regulating the synthesis and transport of bile acid, maintaining systemic energy homeostasis and integrating crosstalk between different organs.<sup>[1-3]</sup> FXR has been considered as a promising target for the treatment of various metabolic disorders, such as cholestatic disorders, fatty liver diseases, type 2 diabetes, dyslipidemia, obesity, atherosclerosis, and renal diseases.<sup>[4-8]</sup> During the last decades, a lot of efforts have been made for discovering and optimizing potential drug candidates for FXR agonists.<sup>[7, 9]</sup>

The dried rhizomes of *Morinda officinalis* is *Morindae Officinalis Radix*, known as “Ba Ji Tian” in Chinese, which is a traditional Chinese medicine (TCM) initially recorded in “Shennong Ben Cao Jing”.<sup>[10, 11]</sup> It possesses kidney-tonifying, strengthening tendons and bones, removing wind and dehumidification effects, therefore, it has been used for the treatment of impotence, nocturnal emission, reproductive diseases, irregular menstruation, abdomen cramp, osteoarthritis, rheumatic arthralgia, and tendon atrophy.<sup>[10-12]</sup> The phytochemical investigation of *Morinda* species led to the isolation and identification of various secondary metabolites, including mornaphthoates A-F, marinoids A-G, monotropein, asperuloside tetraacetate, asperuloside, asperulosidic acid, and polysaccharides, mono-, and oligosaccharides.<sup>[11-15]</sup> Some of them displayed a series of biological activities, such as anti-tumor, anti-inflammatory, hepatoprotective, anti-depression, and antibacterial effects.<sup>[12-17]</sup>

As our continuous work in the discovery of natural FXR agonists and revealing their potential interactions,<sup>[9, 18]</sup> we found that *M. officinalis* exhibited a significantly agonistic effect towards FXR, therefore, its phytochemical constituent was investigated through the bioactivity-guided method to afford twelve compounds (**Figure 1**), including three new iridoid glycosides morindalins A-C (**1-3**) and nine known compounds (**4-12**). Their structural characterization was performed by HRMS, 1D and 2D NMR, and electronic circular dichroism (ECD) spectra as well as quantum chemical computations. Some of them could activate FXR, and their agonistic effect was confirmed by cell imaging technology. Molecular docking and molecular dynamics (MD) stimulation revealed their action mechanism of the interaction with amino acid residues Leu287, Thr288, and Ser332. This finding suggested that compound **6** could be served as a potential candidate for the development of FXR agonists.

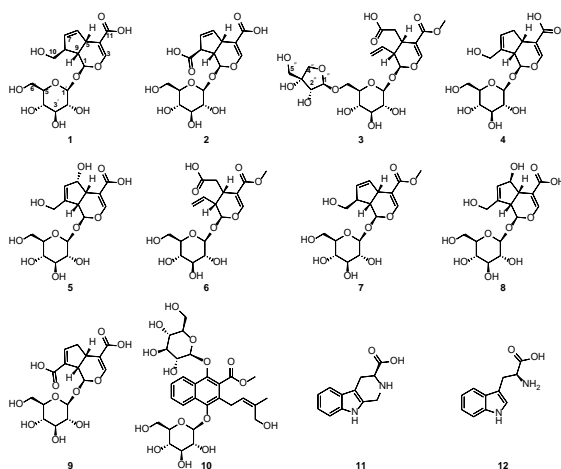


**Figure 1** Chemical structures of compounds **1-12** isolated from *M. officinalis*

## Results and Discussion

### Structural Characterization

Compound **1** was obtained as amorphous powders, and its molecular formula was defined as  $C_{16}H_{22}O_{10}$  according to a quasi-molecular ion peak at  $m/z$  397.1111  $[M + Na]^+$  (calcd. for  $C_{16}H_{22}NaO_{10}$ , 397.1111) in the HRMS spectrum. The  $^1H$  NMR data of **1** (**Table 1**) displayed signals of three olefinic protons at  $\delta_H$  7.47 (1H, d,  $J = 1.5$  Hz, H-3), 5.99 (1H, dt,  $J = 5.7, 2.1$  Hz, H-6), and 5.66 (1H, dt,  $J = 5.7, 2.1$  Hz, H-7), and one anomeric proton at  $\delta_H$  4.66 (1H, d,  $J = 7.9$  Hz, H-1'). The  $^{13}C$  NMR data of **1** (**Table 1**) showed 16 carbon signals, including one carbonyl carbon at  $\delta_C$  170.9 (C-11), four olefinic carbons at  $\delta_C$  153.3 (C-3), 135.9 (C-6), 131.9 (C-7), and 111.8 (C-4), one acetal carbon at  $\delta_C$  97.8 (C-1), and a group of glucose carbons at  $\delta_C$  100.6 (C-1'), 78.4 (C-5'), 78.1 (C-3'), 74.8 (C-2'), 71.6 (C-4'), and 62.7 (C-6'), which suggested that **1** was an iridoid glycoside. The  $^1H$  and  $^{13}C$  NMR data of **1** was closely resembling to those of 8-epiapodantheroside,<sup>[19]</sup> with the following exception that signals of a methoxy group [ $\delta_H$  3.71 (3H, s) and  $\delta_C$  51.7] were absent in **1**, and the chemical shift value of C-11 was shielded from  $\delta_C$  169.1 in 8-epiapodantheroside to  $\delta_C$  170.9 in **1**, revealing that **1** was the derivative of 8-epiapodantheroside. This deduction was confirmed through an HMBC experiment showing long-range correlations of H-3 with C-4/C-5/C-11 (**Figure 2**). In the NOESY spectrum of **1**, correlations of H-9 with H-5/H-10a and H-8 with H-1 (**Figure 3**) suggested an  $\beta$ -orientation of H-1 and  $\beta$ -orientations of H-5, H-9, and hydroxymethyl-8. The glucose linked at C-1 was assigned as  $\beta$ -D-glucose through analysis of the hydrolyzed product of **1** using HPLC with an optical rotation detector<sup>[20]</sup> and the coupling constant [ $\delta_H$  4.66 (1H, d,  $J = 7.9$  Hz, H-1')]. The absolute configuration of **1** was identified through a comparison of calculated and experimental spectra of **1**.<sup>[21, 22]</sup> The calculated ECD of (1*R*,5*S*,8*S*,9*S*)-**1** at the B3LYP/aug-cc-pVDZ level agreed with the experimental spectra of **1**, requiring (1*R*,5*S*,8*S*,9*S*)-configurations (**Figure 4**). Therefore, the structure of **1** was shown in **Figure 1**, and named as morindalin A.

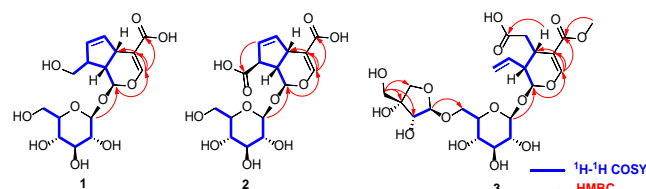


**Figure 2** Selected HMBC and  $^1H$ - $^1H$  COSY correlations of compounds **1-3**.

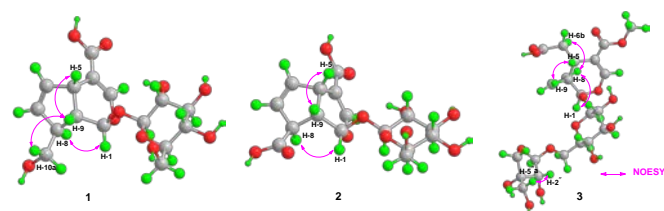


**Figure 3** Selected NOESY correlations of compounds **1-3**.

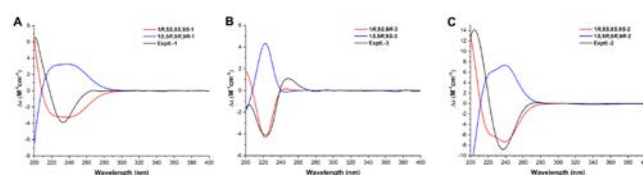


**Figure 4** Experimental and calculated ECD spectra of compounds **1-3** (A-C) at the B3LYP/aug-cc-pVDZ level.

loganin (**6**) found the downfield shift of C-6' from  $\delta_c$  62.7 in secoxyloganin (**6**) to  $\delta_c$  68.8 in **3** and the presence of a suit of an apiose ( $\delta_c$  110.3, 80.7, 78.1, 75.1, and 65.7),<sup>[23]</sup> revealing that this apiose was

**Table 1.**  $^1\text{H}$  (600 MHz,  $\text{CD}_3\text{OD}$ ) and  $^{13}\text{C}$  (150 MHz,  $\text{CD}_3\text{OD}$ ) NMR data of compounds **1-3**

No.	<b>1</b>		<b>2</b>		<b>3</b>	
	$\delta_c$	$\delta_H$ (J in Hz)	$\delta_c$	$\delta_H$ (J in Hz)	$\delta_c$	$\delta_H$ (J in Hz)
1	97.8	5.20 d (5.8)	97.3	5.19 d (5.9)	97.8	5.41 d (4.3)
3	153.3	7.47 d (1.5)	153.5	7.49 d (1.6)	153.8	7.47 d (1.8)
4	111.8		111.4		110.3	
5	41.0	3.62 m	41.3	3.71 m	29.1	3.31 m
6	135.9	5.99 dt (5.7, 2.1)	129.1	5.76 dt (5.6, 2.4)	35.4	2.88 dd (16.4, 5.0) 2.29 dd (16.4, 9.0)
7	131.9	5.66 dt (5.7, 2.1)	137.0	6.07 dt (5.6, 2.4)	176.4	
8	51.5	2.90 m	53.5	3.60 m	134.6	5.64 ddd (17.3, 10.2, 9.6)
9	44.6	2.34 ddd (7.9, 5.7, 4.7)	44.8	2.83 ddd (7.7, 6.1, 4.8)	45.5	2.88 ddd (7.7, 6.1, 4.8)
10	65.3	3.60 m 3.58 m	176.4		120.8	5.28 dd (17.3, 1.7) 5.24 dd (10.2, 1.7)
11	170.9		170.5		169.0	
1'	100.6	4.66 d (7.9)	100.7	4.66 d (7.9)	100.2	4.64 d (7.9)
2'	74.8	3.22 m	74.8	3.24 m	74.7	3.20 dd (9.1, 7.9)
3'	78.1	3.38 m	78.1	3.37 m	78.1	3.35 m
4'	71.6	3.30 m	71.6	3.31 m	71.7	3.29 m
5'	78.4	3.29 m	78.5	3.29 m	77.4	3.44 m
6	62.7	3.86 dd (11.8, 1.8) 3.68 dd (11.8, 5.4)	62.7	3.86 dd (12.1, 2.2) 3.69 dd (12.1, 5.4)	68.8	4.00 d (11.3, 1.9) 3.63 dd (11.3, 6.3)
1''					110.3	5.01 d (2.6)
2''					78.1	3.91 d (2.6)
3''					80.7	
4''					75.1	3.97 d (9.6) 3.77 d (9.6)
5''					65.7	3.57 s
OCH <sub>3</sub> -11					5.18	3.68 s

Compound **2** was isolated as amorphous powders, and has a molecular formula of  $\text{C}_{16}\text{H}_{20}\text{O}_{11}$  based on its HRMS data ( $m/z$  387.0938 [ $\text{M} - \text{H}$ ]<sup>-</sup>, calcd. for  $\text{C}_{16}\text{H}_{19}\text{O}_{11}$ , 387.0927). A detailed comparison of  $^1\text{H}$  and  $^{13}\text{C}$  NMR data of **2** and **1** suggested that their difference was at C-10. The signals of the hydroxymethyl group at C-10 [ $\delta_H$  3.60 (m) and 3.58 (m);  $\delta_C$  65.3] were absent in **2**, and the signal of a carbonyl group ( $\delta_C$  170.5) was present in **2**, indicating that **2** was a C-10 oxidate of **1**. In the HMBC spectrum of **2**, the correlation of H-7 with C-10 (**Figure 2**) verified the above-mentioned deduction. Furthermore, **2** had a  $D$ -glucose with a  $\beta$ -oriented glycosidic bond according to the analysis of its hydrolyzed product by HPLC-OR and the coupling constant [ $\delta_H$  4.66 (1H, d,  $J = 7.9$  Hz, H-1')]. The  $\beta$ -orientations of H-5, H-9, and COOH-10 and an  $\alpha$ -orientation of H-1 were determined based on NOESY cross-peaks of H-1 with H-8 and H-5 with H-9 (**Figure 3**). The absolute configuration of **2** was defined as 1*S*,5*S*,9*R* since the calculated ECD spectrum of 1*S*,5*S*,9*R*-**2** was similar to its experimental result (**Figure 4**). Accordingly, the structure of **2** was shown in **Figure 1**, and named as morindalin B.

The molecular formula of **3** was assigned as  $\text{C}_{22}\text{H}_{32}\text{O}_{15}$  due to its HRMS data ( $m/z$  559.1643 [ $\text{M} + \text{Na}$ ]<sup>+</sup>, calcd. for  $\text{C}_{22}\text{H}_{32}\text{NaO}_{15}$ , 559.1639). Comparison of the  $^1\text{H}$  and  $^{13}\text{C}$  NMR data of **3** and secoxy-

linked at C-6' via a  $\beta$ -oriented glycosidic bond as the coupling constant of the anomeric proton ( $\delta_H$  5.01, d,  $J = 2.6$  Hz, H-1''). This deduction was confirmed by an HMBC correlation of H-1'' with C-6' (**Figure 2**). The configuration of this apiose was determined as  $D$ -configuration according to a NOESY correlation of H-2'' with H-5a'' (**Figure 3**) as previously described.<sup>[24-26]</sup> The (1*R*,5*S*,8*S*,9*S*)-configuration of **3** was assigned due to the agreement of the calculated ECD spectrum of 1*R*,5*S*,8*S*,9*S*-**3** and its experimental result (**Figure 4**). Thus, the structure of **3** was defined as shown in **Figure 1**, and named as morindalin C.

Additionally, nine known compounds (**4-12**) were also isolated from *M. officinalis*, namely geniposidic acid (**4**),<sup>[27]</sup> deacetylasperulosidic acid (**5**),<sup>[28]</sup> secoxyloganin (**6**),<sup>[23]</sup> apodantheroside (**7**),<sup>[29]</sup> scandoside (**8**),<sup>[30]</sup> ixoside (**9**),<sup>[31]</sup> morinlongoside A (**10**),<sup>[32]</sup> 1,2,3,4-tetrahydro- $\beta$ -carboline-3-carboxylic acid (**11**),<sup>[33]</sup> and tryptophane (**12**),<sup>[34]</sup> respectively.

### The agonistic effects of all the isolated compounds towards FXR

All the isolated compounds were assayed for their agonistic effects of towards FXR examined by luciferase assay using FXR gene promoter-driven element luciferase (FXRE) reporter, and the result

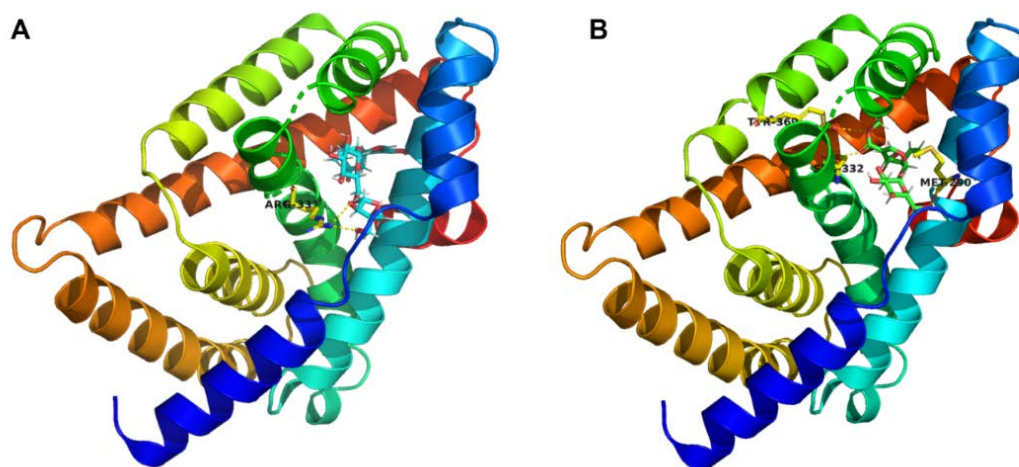


**Figure 5** 3D structures of compounds **3** (A) and **6** (B) with FXR.

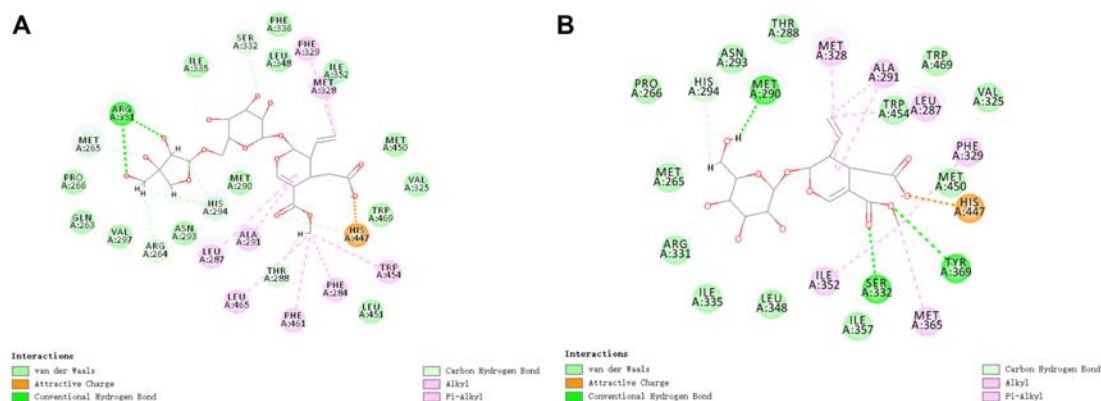


**Figure 6** 2D interactions of compounds **3** (A) and **6** (B) with FXR.

was listed in **Table 2**. Compounds **3** and **6** displayed significant agonistic activities against FXR with  $EC_{50}$  values of 36.48  $\mu\text{M}$  and 7.18  $\mu\text{M}$ , respectively. It should be noted that compounds **1-9** are iridoid glycosides chemically, and while their activities show remarkable differences. A preliminary conclusion regarding the structure-activity relationship (SAR) can be drawn that the *seco*-type iridoids (**3** and **6**) showed a better agonistic effect on FXR than their analogues.

### Molecular docking

In order to reveal their potential interaction with FXR, the 3D structure of FXR was downloaded from Protein Data Bank (<http://www.rcsb.org/structure/3BEJ>, ID 3BEJ), followed by the molecular docking analysis (**Figures 5** and **6**). Compound **3** bond in the ligand-binding domain of FXR through the interaction of van der Waals, attractive charge, hydrogen bond, alkyl, and  $\pi$ -alkyl. Amino acid residue Arg331 interacted with compound **3** via two conventional hydrogen bonds (**Figure 6A**). As shown in **Figure 5B**, compound **6** also bond in the ligand-binding domain of FXR through similar interactions described as compound **3**. Both **3** and **6** possessed a terminal olefinic bond that formed multiple interactions with FXR, which partly explains why *seco*-type iridoids are more active than common analogues. Furthermore, it was worth noting that three conventional hydrogen bonds of amino acid residues Met290, Ser332, and Tyr369 with compound **6** were observed in **Figure 6B**.

These results reveal the reason at the molecular level why the agonistic effect of compound **6** was more potent than that of compound **3**.

**Table 2.** The agonistic effects of compounds **1-12** against FXR.

Compound	$EC_{50}$ ( $\mu\text{M}$ )	Compound	$EC_{50}$ ( $\mu\text{M}$ )
<b>1</b>	> 100	<b>7</b>	> 100
<b>2</b>	> 100	<b>8</b>	> 100
<b>3</b>	36.48	<b>9</b>	> 100
<b>4</b>	> 100	<b>10</b>	> 100
<b>5</b>	> 100	<b>11</b>	> 100
<b>6</b>	7.18	<b>12</b>	> 100

### Molecular dynamics stimulation

The potential interaction of compound **6** with FXR was analyzed by molecular docking, revealing that amino acid residues played a crucial role in the activation of compound **6** towards FXR. To elucidate how they changed during 50 ns of MD stimulation, the final docking result was applied for the investigation of the dynamical interaction of compound **6** with FXR (**Figure 7**). During 50 ns of MD stimulation, RMSD remained under 2  $\text{\AA}$  (**Figure 7A**) that was an important parameter for the evaluation of the stability of ligand with protein, the radius of gyration of compound **6** with FXR remained at the distance of 1.3-1.6 nm at three degrees of freedom (X, Y, and

Z axes, **Figure 7C**), and RMSF of residues was acquired to figure out regions exhibiting higher flexibility with a distance of 1–5 Å (**Figure 7B**). These results indicated the reliability of the MD stimulation between compound **6** and FXR. The potential energy of the complex of compound **6** with FXR was about  $-5.85 \times 10^5$  kJ/mol (**Figure 7D**).

towards FXR, therefore, we investigated the mRNA and protein levels of the well-known downstream targets of FXR in the liver (SHP1 and BSEP) and kidney (OST $\alpha$  and OST $\beta$ ) after administration of compound **6** (10  $\mu$ M for 24 h) in HepG2 and HK2. CDCA, a defined FXR agonist, was used as a positive control (40  $\mu$ M for 24 h). After the

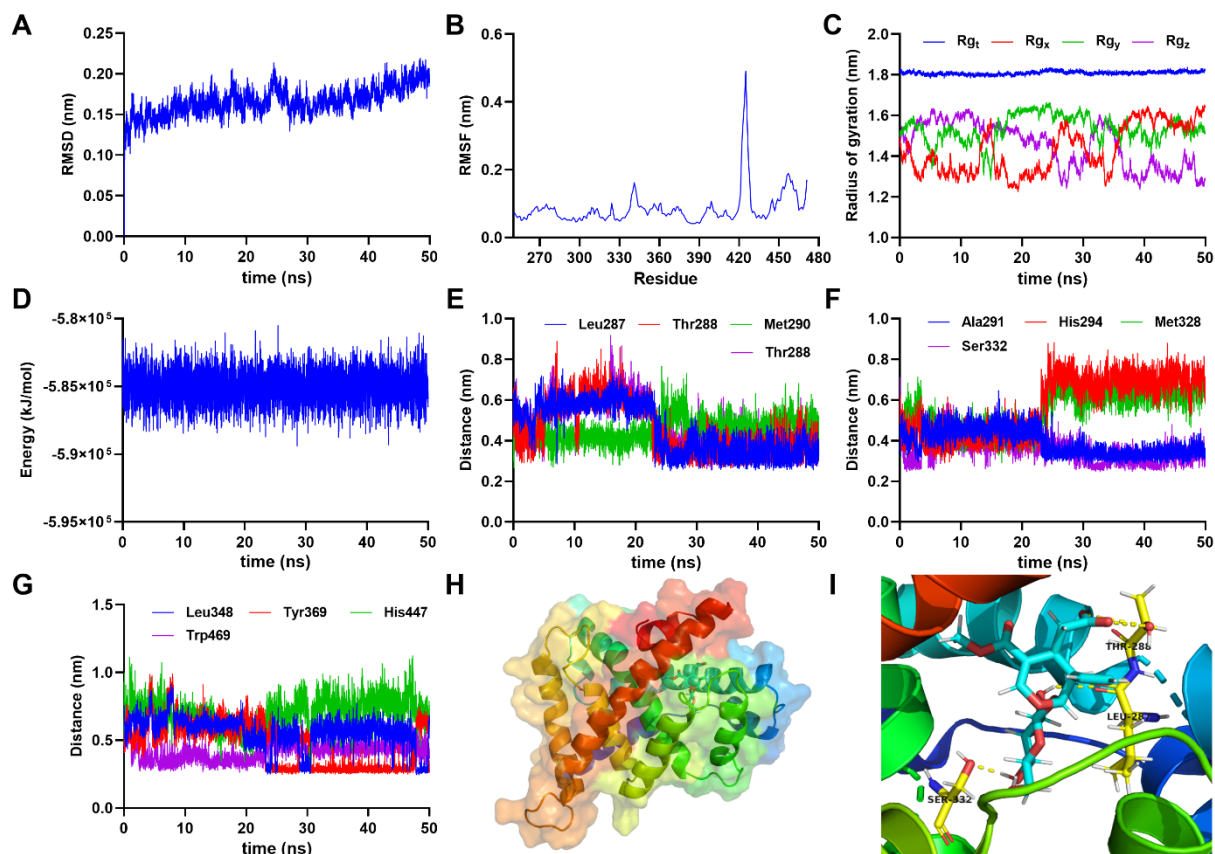


**Figure 7** (A) RMSD of compound **6** with FXR for 50 ns of MD stimulation. (B) RMSF of compound **6** with FXR for 50 ns of MD stimulation. (C) Radius of gyration of compound **6** with FXR for 50 ns of MD stimulation. (D) The potential energy of compound **6** with FXR for 50 ns of MD stimulation. (E) The distance of compound **13** with amino acid residues Leu287, Thr288 (two hydrogen bonds), and Met290. (F) The distance of compound **6** with amino acid residues Ala291, His294, Met328, and Ser332. (G) The distance of compound **6** with amino acid residues Leu348, Tyr369, His447, and Trp469. (H) 3D structure of compound **6** with FXR at 50<sup>th</sup> ns of MD stimulation. (I) The interaction of compound **6** with amino acid residues Leu287, Thr288, and Ser332 *via* four hydrogen bonds at 50<sup>th</sup> ns of MD stimulation.

Compared with the result of molecular docking, eleven amino acid residues Leu287, Thr288, Met290, Ala291, His294, Met328, Ser332, Leu348, Tyr369, His447, and Trp469 could form twelve hydrogen bonds with compound **6** during 50 ns of MD stimulation (**Figure 7E–G**), whereas some of the hydrogen bond interactions were unstable, including Met290, Ala291, His294, Met328, Leu348, Tyr369, His447, and Trp469, because their distances with compound **6** were more than 3.5 Å that was an acceptable distance to form a hydrogen bond. As same as described in molecular docking, compound **6** could still bind to the Ligand binding domain of FXR through four hydrogen bonds between the hydroxy group of Thr288 and COOH-7 of compound **6**, the carbonyl group of Leu287 and OH-2' of compound **6**, and the hydroxy group of Ser332 and OH-4' of compound **6** during this MD stimulation. These findings clarified that compound **6** could activate FXR through the interactions with amino acid residues Leu287, Thr288, and Ser332, indicating that compound **6** could be regarded as an agent for the development of FXR agonists.

#### Induction of FXR downstream targets by compound **6**

Compound **6** displayed the most significantly agonistic effect

treatment with compound **6**, the mRNA levels of SHP1, BSEP, OST $\alpha$ , and OST $\beta$  were all significantly up-regulated (**Figure 8A**). In parallel, the protein levels of these FXR targets were also increased by compound **6** (**Figure 8B–C**). To further confirm whether the transcriptional regulation of FXR was modulated by compound **6**, the cellular location of FXR was observed in HepG2 cells. After the administration of compound **6**, the cells showed clear translocation of FXR from cytoplasm to nucleus (**Figure 9**). These results indicated that compound **6** could activate FXR and transcriptionally regulated the expression of FXR downstream targets, suggesting that compound **6** could serve as a candidate for the development of FXR agonists.

#### Conclusions

In summary, the investigation of *M. officinalis* resulted in the isolation and identification of three new iridoid glycosides morindalins A–C (**1–3**) and nine known compounds (**4–12**). Compound **6** displayed significantly agonistic activities against FXR with an EC<sub>50</sub> value of 7.18  $\mu$ M. The result of cell imaging technology clarified their agonistic effect against FXR at the cell level. Molecular docking and MD stimulation revealed their action mechanism through the

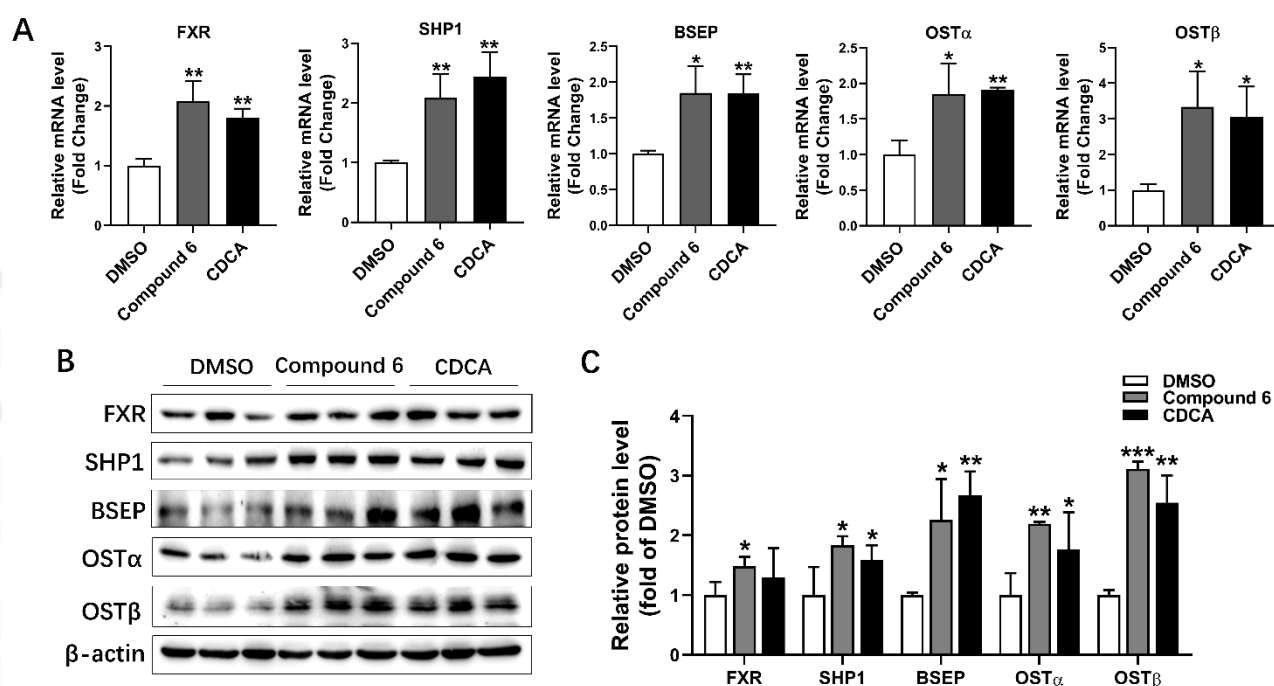


**Figure 8** Effect of compound **6** on FXR and its downstream target genes. (A) qPCR analysis showing the induction of FXR and its renal downstream targets (SHP1, BSEP, OST $\alpha$ , and OST $\beta$ ) in HepG2 cells treated with compound **6** (10  $\mu$ M for 24 h). CDCA (40  $\mu$ M for 24 h) was used as a positive control. (B) Western blot analysis demonstrating a significant increase in the protein levels of FXR and its downstream targets in HepG2 cells treated with compound **6**. (C) Quantitative analysis of western blot results for FXR and its downstream targets in renal cells treated with compound **6**. Data represent the mean  $\pm$  SD,  $n = 3$  for each group. \* $p < 0.05$ , \*\* $p < 0.01$ , \*\*\* $p < 0.001$  compared to the DMSO group.

hydrogen bond interaction with amino acid residues Leu287, Tyr288, and Ser332. These findings suggested that compound **6** could be regarded as a potential candidate for the development of FXR agonists.

## Experimental

### General Experimental Procedures

The optical rotations of isolated compounds were recorded on a Jasco J-715 polarimeter. ECD spectra were recorded on a Bio-Logic Science MOS-450 spectrometer. 1D and 2D NMR data were recorded on a Bruker AV-600 spectrometer. Chemical shift values are expressed in  $\delta$  (ppm) using the peak signals of the solvent CD<sub>3</sub>OD ( $\delta_{\text{H}}$  3.31 and  $\delta_{\text{C}}$  49.2) as references, and coupling constants ( $J$  in Hz) are given in parentheses. The antibody of FXR (PP-9033A-00) was purchased from R&D Systems. The antibodies of small heterodimer partner 1 (SHP1, ab32559), and organic solute transporter subunit beta (OST $\beta$ , ab121285) were purchased from Abcam. The antibody of bile salt export pump (BSEP, A8467) was purchased from Abclonal. The antibody of organic solute transporter subunit alpha (OST $\alpha$ , bs-17529R) was purchased from BLOSS.

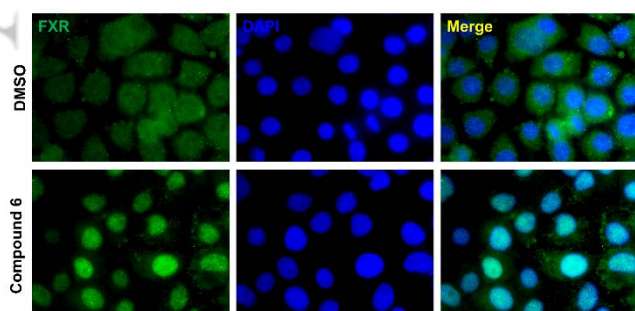


**Figure 9** Nuclear translocation of FXR stimulated by compound **6**.

### Plant Material

Dried rhizomes of *M. officinalis* were purchased from Beijing Tongrentang Co., Ltd. (Dalian, China) in June 2020, and identified by Prof. Jing-Ming Jia (Shenyang Pharmaceutical University). A voucher specimen (MO202006) has been deposited in the Department of Medicinal Chemistry, Dalian Medical University.

### Extraction and Isolation

*M. officinalis* (800 g) was extracted with 90% EtOH (8 L) for three times to obtain a residue after removing the solvent. The residue was suspended by 2 L water, and extracted with ethyl acetate (3  $\times$  2 L), and *n*-BuOH (3  $\times$  2 L), respectively.

The *n*-BuOH extract (10 g) was separated by a silica gel (Qingdao Marine Chemical Factory, Qingdao, China) column and eluted with CH<sub>2</sub>Cl<sub>2</sub>-MeOH (from 50:1 to 1:1), resulting in the production of eight fractions B1-B8. B5 (536 mg) was purified through preparative HPLC with a YMC C<sub>18</sub> column (250 mm  $\times$  10 mm, 5  $\mu$ m) and eluted with 10%-70% MeOH to afford three subfractions B51-B53. Separation of B53 (82 mg) through preparative HPLC (15% MeCN) led to the isolation of compounds **3** (4.7 mg), **6** (4.9 mg), and **7** (2.7 mg). Compounds **4** (1.7 mg), **5** (12.6 mg), and **8** (21 mg) were isolated from B6 (120 mg) through preparative HPLC (10%-70% MeOH). B7 (523 mg) was separated by preparative HPLC (10%-70% MeOH), which was further purified by preparative HPLC (10%-20% MeOH) to afford compounds **1** (3.7 mg), **2** (4.0 mg), **9** (4.8 mg), and **10** (5.0 mg). Finally, separation of B8 (135 mg) through preparative HPLC (10%-70% MeOH) afforded compounds **11** (3.4 mg) and **12** (4.3 mg).

**Morindalin A (1):** amorphous powder;  $[\alpha]_{\text{D}}^{20} -16$  (c 0.1, MeOH); UV (MeOH)  $\lambda_{\text{max}}$  (log  $\epsilon$ ) 240 (3.8) nm; ECD (MeOH) nm ( $\Delta\epsilon$ ) 201 (+6.57), 233 (-3.88); <sup>1</sup>H (600 MHz, CD<sub>3</sub>OD) and <sup>13</sup>C NMR (150 MHz, CD<sub>3</sub>OD) data, see Table 1; HRMS  $m/z$  397.1111 [M + Na]<sup>+</sup> (calcd. for C<sub>16</sub>H<sub>22</sub>NaO<sub>10</sub>, 397.1111).

**Morindalin B (2):** amorphous powder;  $[\alpha]_{\text{D}}^{20} -13$  (c 0.1, MeOH); UV (MeOH)  $\lambda_{\text{max}}$  (log  $\epsilon$ ) 237 (3.7) nm; ECD (MeOH) nm ( $\Delta\epsilon$ ) 204

(+14.14), 237 (−8.81);  $^1\text{H}$  (600 MHz,  $\text{CD}_3\text{OD}$ ) and  $^{13}\text{C}$  NMR (150 MHz,  $\text{CD}_3\text{OD}$ ) data, see **Table 1**; HRMS  $m/z$  387.0938  $[\text{M} - \text{H}]^-$  (calcd. for  $\text{C}_{16}\text{H}_{19}\text{O}_{11}$ , 387.0927).

*Morindalin C* (**3**): amorphous powder;  $[\alpha]_{\text{D}}^{20}$  −74 (c 0.1, MeOH); UV (MeOH)  $\lambda_{\text{max}}$  (log  $\epsilon$ ) 237 (3.6) nm; ECD (MeOH) nm ( $\Delta\epsilon$ ) 223 (−4.13), 319 (+1.10);  $^1\text{H}$  (600 MHz,  $\text{CD}_3\text{OD}$ ) and  $^{13}\text{C}$  NMR (150 MHz,  $\text{CD}_3\text{OD}$ ) data, see **Table 1**; HRMS  $m/z$  559.1643  $[\text{M} + \text{Na}]^+$  (calcd. for  $\text{C}_{22}\text{H}_{32}\text{NaO}_{15}$ , 559.1639).

### ECD Calculations

To save consumption of calculations, model compounds with the glycosyl units replaced with methyl groups were used for the ECD calculations.<sup>[35, 36]</sup> The conformation search of compounds **1-3** was carried out at Merck Molecular Force Field (MMFF) by Discovery Studio software, and the low energy conformers were kept with a low energy cutoff of < 5 kcal/mol.<sup>[21, 22]</sup> Geometries were optimized using DFT at B3LYP/6-31G(d) level within a MeOH solvent simulated using Gaussian 09 package (Gaussian 09, 2009). Harmonic vibrational frequencies were also calculated at the same level of theory to ensure that no imaginary values were present, confirming that all the conformers were stable. The ECD calculations were run with B3LYP functional and the aug-cc-pVDZ basis set of Gaussian 09 package with the same solvent as in the preceding DFT optimization step. Depended on the Boltzmann distribution, the final ECD spectra of compounds **1-3** were obtained by weighting spectra of all conformers.

### The determination of the glycoside of compounds 1-3

The absolute configurations of the glycoside of compounds **1-3** were determined by HPLC-OR as previously described.<sup>[20]</sup> Compounds **1-3** (1 mg) was hydrolyzed by 2M HCl (2.0 mL) at 90 °C for 4 h to obtain the monosaccharide in the aqueous layer after the  $\text{CHCl}_3$  extraction, and analyzed by HPLC with a Jasco LC-NetII/ADC system.

### Molecular docking

The 3D structure of FXR was downloaded from Protein Data Bank (<http://www.rcsb.org/structure/3BEJ>, ID 3BEJ), and then was used to study the interactions between compounds **3** or **6** and FXR by Discovery Studio 2016 (Accelrys, CA, USA).<sup>[9]</sup> Firstly, the energy optimization of 3D structures of compounds **3** and **6** was performed with the CHARMM force field using the module of Prepare Ligand (Discovery Studio 2016). The active pocket for substrate binding was defined based on the site of the crystallographic ligand MFA-1. The interaction of compound **6** with FXR was calculated by the module of CDOCKER (Discovery Studio 2016), and the 3D interaction was plotted by PyMOL software.

### Molecular dynamics stimulation

GROMACS package was applied to study MD simulation at the AMBER99SB force field.<sup>[37, 38]</sup> The restrained electrostatic potential charges of ligand were performed at HF/6-31G\* level using Gaussian 09 program. The starting topology of the ligand was generated by antechamber and ACPYPE programs. The best docking pose was subjected to the steepest descent energy minimization to relax the system. Then, NVT and NPT were used to equilibrate the minimized system at the constant temperature of 300 K and the constant pressure of 1 bar, respectively. In the last step, 50 ns of MD simulation at 300 K and 1 bar pressure was performed, thus carrying out the interaction analyses between the enzyme and ligand. The trajectory file was analyzed by GROMACS to produce the root mean square deviation (RMSD), root mean square fluctuations (RMSF), and other parameters. The MD results were plotted by PyMOL and GraphPad prism software.

### Cell Culture

The human liver hepatocellular cells (HepG2) were cultured in

DMEM medium containing 10% fetal bovine serum (FBS). Human proximal tubular epithelial cells (HK2) were maintained in DMEM/F12 medium supplemented with 10% FBS. Cells were all placed in an incubator at 37 °C and maintained in a humidified atmosphere containing 5%  $\text{CO}_2$ .

### FXR activation bioassay

The human FXR cDNA was cloned and inserted into pcDNA3.1 for the construction of FXR overexpression vector.<sup>[9]</sup> FXRE reporter was constructed by cloning a genomic DNA fragment upstream bile salt export pump (BSEP) promoter into the luciferase vector pGL3.0-basic. The human hepatoma HepG2 cell line was transiently transfected with the expression plasmid of FXR, FXRE reporter, and the null-Renilla luciferase plasmid as an internal control. After 24 h, cells were treated with vehicle DMSO (0.1%) or corresponding compounds at different concentrations. The cells were then harvested for the determination of luciferase activity by Dual-Luciferase® Reporter Assay System (E1960, Promega, Madison, WI, USA).

### RNA isolation and real-time quantitative PCR

Total RNA was isolated from HepG2 and HK2 cells by the RNeasy Mini Kit (Qiagen, Germany), and quantified according to the manufacturer's instructions. The quantity and purity of the extracted RNA were examined by using a Nanodrop spectrophotometer (Thermo, USA). Reverse transcription was performed by reverse transcription kit (Tiangen, Beijing, China). The cDNA was used as a template for real-time quantitative PCR on the Rism 7500 real-time PCR instrument with TransStart Tip Green qPCR SuperMix (Transgen, China). Primer was designed by Software Oligo 6.0 (MBI Inc., Colorado, USA) (**Table S1**).

### Western Blot

Cells were dissolved in RIPA Lysis buffer (Merck, Germany) with protease inhibitor cocktail (Sigma-Aldrich, China), and then the supernatants were collected. The concentrations of the protein samples were examined by bicinchoninic acid protein assay kit (Sigma-Aldrich, China). Samples were heated for denaturation in the loading buffer for 10 min at 95 °C. The denatured samples were then separated by 10 % SDS-polyacrylamide gel electrophoresis (SDS-PAGE), and transferred to polyvinylidene difluoride (PVDF) membranes (Millipore, USA) which were then blocked with 10% (w/v) skim milk and subsequently incubated with selected primary antibodies overnight at 4 °C. After washes, the membranes were incubated for 1 h at room temperature with HRP-conjugated secondary antibodies. After washes, staining was developed using Tanon 5200 ECL detection system (Tanon, China).

### Immunohistochemistry

Cells were firstly fixed with 4% PFA in PBS. After washed with ice-cold PBS, cells were permeabilized with 0.3% Triton X-100 in PBS for 10 min and blocked by 0.5% BSA in PBS for 30 mins. The cells were then incubated with primary antibody overnight at 4 °C. After washes, the cells were incubated with appropriate Dylight 488 (green) conjugated secondary antibody (Jackson Immuno Research Laboratories) for 1 h at room temperature. Nuclei were stained with DAPI. Images were obtained through a confocal microscope.

### Supporting Information

The supporting information for this article is available on the WWW under <https://doi.org/10.1002/cjoc.2021xxxx>.

### Acknowledgement

This work was supported by National Natural Science Foundation of China (No. 81703679), Liaoning Provincial Key Research and Development Program (2019JH2/10300022), Natural Science Foundation of Liaoning Province (2020-MS-256), and Dalian Young Star of Science and Technology.

## References

- Forman, B.M.; Goode, E.; Chen, J.; Oro, A.E.; Bradley, D.J.; Perlmann, T.; Noonan, D.J.; Burka, L.T.; McMorris, T.; Lamph, W.W.; Evans, R.M.; Weinberger, C. Identification of a nuclear receptor that is activated by farnesol metabolites. *Cell*. **1995**, *81*, 687-693.
- Lee, F.Y.; Lee, H.; Hubbert, M.L.; Edwards, P.A.; Zhang, Y. FXR, a multi-purpose nuclear receptor. *Trends Biochem Sci*. **2006**, *31*, 572-580.
- Sinal, C.J.; Tohkin, M.; Miyata, M.; Ward, J.M.; Lambert, G.; Gonzalez, F.J. Targeted disruption of the nuclear receptor FXR/BAR impairs bile acid and lipid homeostasis. *Cell*. **2000**, *102*, 731-744.
- Chavez-Talavera, O.; Tailleux, A.; Lefebvre, P.; Staels, B. Bile Acid Control of Metabolism and Inflammation in Obesity, Type 2 Diabetes, Dyslipidemia, and Nonalcoholic Fatty Liver Disease. *Gastroenterology*. **2017**, *152*, 1679-1694 e1673.
- Levi, M. Nuclear receptors in renal disease. *Biochim. Biophys. Acta*. **2011**, *1812*, 1061-1067.
- Moris, D.; Giaginis, C.; Tsourouflis, G.; Theocharis, S. Farnesoid-X Receptor (FXR) as a Promising Pharmaceutical Target in Atherosclerosis. *Curr. Med. Chem*. **2017**, *24*, 1147-1157.
- Sepe, V.; Distrutti, E.; Fiorucci, S.; Zampella, A. Farnesoid X receptor modulators 2014-present: a patent review. *Expert Opin. Ther. Pat*. **2018**, *28*, 351-364.
- Teodoro, J.S.; Rolo, A.P.; Palmeira, C.M. Hepatic FXR: key regulator of whole-body energy metabolism. *Trends Endocrinol. Metab*. **2011**, *22*, 458-466.
- Luan, Z.L.; Huo, X.K.; Dong, P.P.; Tian, X.G.; Sun, C.P.; Lv, X.; Feng, L.; Ning, J.; Wang, C.; Zhang, B.J.; Ma, X.C. Highly potent non-steroidal FXR agonists protostane-type triterpenoids: Structure-activity relationship and mechanism. *Eur. J. Med. Chem*. **2019**, *182*, 111652.
- Singh, B.; Sharma, R.A. Indian *Morinda* species: A review. *Phytother. Research*. **2020**, *34*, 924-1007.
- Zhang, J.H.; Xin, H.L.; Xu, Y.M.; Shen, Y.; He, Y.Q.; Hsien-Yeh; Lin, B.; Song, H.T.; Juan-Liu; Yang, H.Y.; Qin, L.P.; Zhang, Q.Y.; Du, J. *Morinda officinalis* How. - A comprehensive review of traditional uses, phytochemistry and pharmacology. *J. Ethnopharmacol*. **2018**, *213*, 230-255.
- Yu, J.H.; Zhai, H.J.; Yu, Z.P.; Zhang, Q.Q.; Ge, Y.X.; Zhang, Y.Y.; Jiang, C.S.; Zhang, H. Methyl 2-naphthoates from a traditional Chinese herb *Morinda officinalis* var. *officinalis*. *Tetrahedron*. **2019**, *75*, 3793-3801.
- Xu, H.L.; Liu, L.L.; Chen, Y.X.; Ma, H.; Li, M.; Qu, W.S.; Yin, J.; Zhang, X.; Gao, Y.T.; Shan, J.J.; Gao, Y.Q. The chemical character of polysaccharides from processed *Morinda officinalis* and their effects on anti-liver damage. *Int. J. Biol. Macromol*. **2019**, *141*, 410-421.
- Zhai, H.J.; Ye, G.H.; Xue, J.J.; Yu, J.H.; Zhang, Y.Y.; Zhang, H. Two new naphthoate derivatives from *Morinda officinalis*. *J. Asian Nat. Prod. Res*. **2019**.
- Zhai, H.J.; Yu, J.H.; Zhang, Q.Q.; Liu, H.S.; Zhang, J.S.; Song, X.Q.; Zhang, Y.Y.; Zhang, H. Cytotoxic and antibacterial triterpenoids from the roots of *Morinda officinalis* var. *officinalis*. *Fitoterapia*. **2019**, *133*, 56-61.
- Jiang, K.M.; Huang, D.; Zhang, D.W.; Wang, X.L.; Cao, H.J.; Zhang, Q.; Yan, C.Y. Investigation of inulins from the roots of *Morinda officinalis* for potential therapeutic application as anti-osteoporosis agent. *Int. J. Biol. Macromol*. **2018**, *120*, 170-179.
- Yan, C.Y.; Huang, D.; Shen, X.; Qin, N.B.; Jiang, K.M.; Zhang, D.W.; Zhang, Q. Identification and characterization of a polysaccharide from the roots of *Morinda officinalis*, as an inducer of bone formation by up-regulation of target gene expression. *Int. J. Biol. Macromol*. **2019**, *133*, 446-456.
- Huo, X.K.; Liu, J.; Yu, Z.L.; Wang, Y.F.; Wang, C.; Tian, X.G.; Ning, J.; Feng, L.; Sun, C.P.; Zhang, B.J.; Ma, X.C. *Alisma orientale* extract exerts the reversing cholestasis effect by activation of farnesoid X receptor. *Phyto-medicine*. **2018**, *42*, 34-42.
- Machida, K.; Takehara, E.; Kobayashi, H.; Kikuchi, M. Studies on the constituents of *Gardenia* species. III. New iridoid glycosides from the leaves of *Gardenia jasminoides* cv. *fortuneana* Hara. *Chem. Pharm. Bull. (Tokyo)*. **2003**, *51*, 1417-1419.
- Sun, C.P.; Yuan, T.; Wang, L.; Kang, N.; Zhao, F.; Chen, L.X.; Qiu, F. Anti-inflammatory labdane-type diterpenoids from *Physalis angulata*. *Rsc Adv*. **2016**, *6*, 76838-76847.
- Liang, J.H.; Luan, Z.L.; Tian, X.G.; Zhao, W.Y.; Wang, Y.L.; Sun, C.P.; Huo, X.K.; Deng, S.; Zhang, B.J.; Zhang, Z.J.; Ma, X.C. Uncarialsins A-I, Monoterpenoid Indole Alkaloids from *Uncaria rhynchophylla* as Natural Agonists of the 5-HT<sub>1A</sub> Receptor. *J. Nat. Prod*. **2019**, *82*, 3302-3310.
- Wang, C.; Huo, X.K.; Luan, Z.L.; Cao, F.; Tian, X.G.; Zhao, X.Y.; Sun, C.P.; Feng, L.; Ning, J.; Zhang, B.J.; Ma, X.C. Alismanin A, a Triterpenoid with a C34 Skeleton from *Alisma orientale* as a Natural Agonist of Human Pregnane X Receptor. *Org. Lett*. **2017**, *19*, 5645-5648.
- Hiroshi, K.; Masami, M.; Kiyokazu, T.; Kenichiro, I.; Tetsuro, F.; He, Z.D.; Yang, C.R. Secoiridoid, coumarin and secoiridoid-coumarin glucosides from *Fraxinus chinensis*. *Phytochemistry*. **1992**, *31*, 1277-1280.
- Peng, K.; Yang, L.; Zhao, S.; Chen, L.; Zhao, F.; Qiu, F. Chemical constituents from the fruit of *Gardenia jasminoides* and their inhibitory effects on nitric oxide production. *Bioorg. Med. Chem. Lett*. **2013**, *23*, 1127-1131.
- Takayanagi, T.; Ishikawa, T.; Kitajima, J. Sesquiterpene lactone glucosides and alkyl glycosides from the fruit of cumin. *Phytochemistry*. **2003**, *63*, 479-484.
- Zhou, K.; Zhao, F.; Liu, Z.; Zhuang, Y.; Chen, L.; Qiu, F. Triterpenoids and flavonoids from celery (*Apium graveolens*). *J. Nat. Prod*. **2009**, *72*, 1563-1567.
- Tao, S.H.; Wu, J.; Qi, S.H.; Zhang, S.; Li, M.Y.; Li, Q.X. Scyphiphorins A and B, two new iridoid glycosides from the stem bark of a Chinese mangrove *Scyphiphora hydrophyllacea*. *Helv. Chim. Acta*. **2007**, *90*, 1718-1722.
- Esakkimuthu, S.; Nagulkumar, S.; Darvin, S.S.; Buvanavaragurunathan, K.; Sathya, T.N.; Navaneethakrishnan, K.R.; Kumaravel, T.S.; Murugan, S.S.; Shirota, O.; Balakrishna, K.; Pandikumar, P.; Ignacimuthu, S. Anti-hyperlipidemic effect of iridoid glycoside deacetylasperulosidic acid isolated from the seeds of *Spermacoce hispida* L. - A traditional anti-obesity herb. *J. Ethnopharmacol*. **2019**, *245*.
- Francois, B.; Pierre, D.; Michel, K. Apodantheroside, an iridoid glucoside from *Feretia apodanthera*. *Phytochemistry*. **1980**, *19*, 2763-2764.
- Kohei, K.; Yasuhiro, F.; Yasuhisa, S.; Endang, H.; Umar, M.; Toshiko, S. Studies on the constituents of *Indonesian Borreria latifolia*. *Heterocycles*. **2002**, *56*, 537-544.
- Takeda, Y.; Nishimura, H.; Inouye, H. Two new iridoid glucosides from *Ixora chinensis*. *Phytochemistry*. **1975**, *14*, 2647-2650.
- Cuong, N.M.; Huong, T.T.; Son, N.T.; Cuong, T.D.; Van, D.T.; Khanh, P.N.; Ha, V.T.; Tram, N.C.; Long, P.Q.; Kim, Y.H. Morinlongosides A-C, Two New Naphthalene Glycoside and a New Iridoid Glycoside from the Roots of *Morinda longissima*. *Chem. Pharm. Bull. (Tokyo)*. **2016**, *64*, 1230-1234.
- Xie, G.Y.; Qin, X.Y.; Chen, Y.J.; Wen, R.; Wu, S.S.; Qin, M.J. Alkaloids from the Rhizomes of *Iris germanica*. *Chem. Nat. Compd*. **2017**, *53*, 196-198.
- Lu, H.L.; Ouyang, F.; Su, Y.L.; Ji, T.F.; Liu, H. Study on chemical constituents of the fruits of *Nitraria tangutorum* Bobr. *Northwest Pharm. J*. **2013**, *28* 221-223.
- Tatsis, E.C.; Schaumlöffel, A.; Warskulat, A.C.; Massiot, G.; Schneider, B.; Bringmann, G. Nudicaulins, Yellow Flower Pigments of *Papaver nudicaule*: Revised Constitution and Assignment of Absolute Configuration. *Org. Lett*. **2013**, *15*, 156-159.
- Zhao, W.; Song, X.; Zhao, L.; Zou, C.; Zhou, W.; Lin, B.; Yao, G.; Huang, X.; Song, S. Quassinoids from *Picrasma quassioides* and their neuroprotective effects. *J. Nat. Prod*. **2019**, *82*, 714-723.
- Sun, C.P.; Yan, J.K.; Yi, J.; Zhang, X.Y.; Yu, Z.L.; Huo, X.K.; Liang, J.H.; Ning, J.; Feng, L.; Wang, C.; Zhang, B.J.; Tian, X.G.; Zhang, L.; Ma, X. The study

of inhibitory effect of natural flavonoids toward beta-glucuronidase and interaction of flavonoids with beta-glucuronidase. *Int. J. Biol. Macromol.* **2020**, *143*, 349-358.

- [38] Yun, W.J.; Zhang, X.Y.; Liu, T.T.; Liang, J.H.; Sun, C.P.; Yan, J.K.; Huo, X.K.; Tian, X.G.; Zhang, B.J.; Huang, H.L.; Ma, X.C. The inhibition effect of uncarialin A on voltage-dependent L-type calcium channel subunit alpha-1C: Inhibition potential and molecular stimulation. *Int. J. Biol. Macromol.* **2020**, *159*, 1022-1030.

---

(The following will be filled in by the editorial staff)

Manuscript received: XXXX, 2021

Manuscript revised: XXXX, 2021

Manuscript accepted: XXXX, 2021

Accepted manuscript online: XXXX, 2021

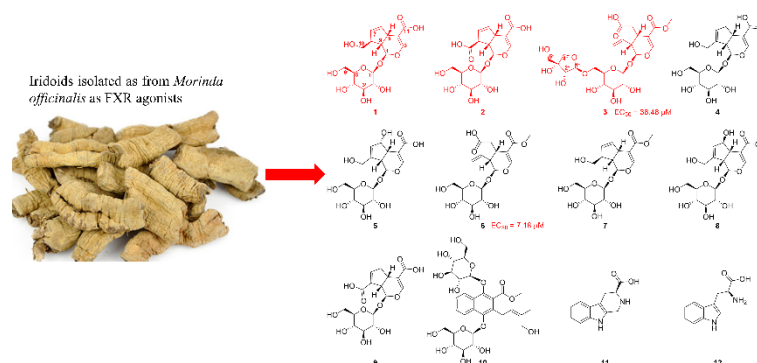
Version of record online: XXXX, 2021

Accepted Article

## Entry for the Table of Contents

Discovery of new iridoids as FXR agonists from *Morinda officinalis*: Agonistic potentials and molecular stimulationsZhi-Lin Luan,<sup>a</sup> Fei Qiao,<sup>a</sup> Wen-Yu Zhao,<sup>a</sup> Wen-Hua Ming, Zhen-Long Yu, Jie Liu, Sheng-Yun Dai, Shuang-Hui Jiang, Chao-Jie Lian, Cheng-Peng Sun,<sup>\*</sup> Bao-Jing Zhang, Jian Zheng,<sup>\*</sup> Shuang-Cheng Ma,<sup>\*</sup> and Xiao-Chi Ma

Chin. J. Chem. 2021, 39, XXX–XXX. DOI: 10.1002/cjoc.202100XXX

New iridoids from Traditional Chinese Medicine *M. officinalis* showed significant agonistic activity against FXR at both gene and protein levels.

<sup>a</sup> Dalian Key Laboratory of Metabolic Target Characterization and Traditional Chinese Medicine Intervention, College of Pharmacy, College of Integrative Medicine, Dalian Medical University, Dalian, China.

<sup>b</sup> National Institutes for Food and Drug Control, Beijing, China